ACS Photonics

pubs.acs.org/journal/apchd5

Article

High-Performance White Light-Emitting Diodes over 150 lm/W Using Near-Unity-Emitting Quantum Dots in a Liquid Matrix

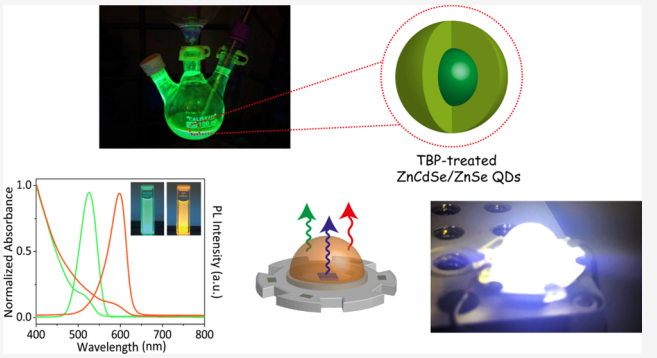
Asim Onal, Guncem Ozgun Eren, Sadra Sadeghi, Rustamzhon Melikov, Mertcan Han, Onuralp Karatum, Melek Sermin Ozer, Houman Bahmani Jalali, Itir Bakis Dogru-Yuksel, Iskender Yilgor, Önder Metin, and Sedat Nizamoglu*

Cite This: *ACS Photonics* 2022, 9, 1304–1314

Read Online

ACCESS | Metrics & More | Article Recommendations | Supporting Information

ABSTRACT: In the next decade, we will witness the replacement of a majority of conventional light sources with light-emitting diodes (LEDs). Efficient LEDs other than phosphors can enhance their functionality and meet different lighting needs. Quantum dots (QDs) have high potential for future LED technology due to their sensitive band-gap tuning via the quantum confinement effect and compositional control, high photoluminescence quantum yield (PLQY), and mass-production capacity. Herein, we demonstrate white LEDs using QDs that reach over 150 lumens per electrical Watt. For that we synthesized green- and red-emitting ZnCdSe/ZnSe core/shell QDs by low-temperature nucleation, high-temperature shell formation, and postsynthetic trap-state removal. Their cadmium concentration is lower than 100 ppm, satisfying the current EU RoHS regulations, and their PLQY reaches a high level of 94%. The PLQY of QDs is maintained within the device on blue LED via liquid injection, and their integration at optimized optical densities leads to 129.6 and 170.4 lm/W for red-green-blue (RGB)- and green-blue (GB)-based white LEDs, respectively. Our simulations further showed that an efficiency level of over 230 lm/W is achievable using ultraefficient blue LED pumps. The simple fabrication and high performance of white LEDs using QD liquids show high promise for next-generation lighting devices.



KEYWORDS: *quantum dot, light-emitting diodes, white light-emitting diodes, quantum efficiency, luminous efficiency, external quantum efficiency*

Downloaded via 78.180.117.39 on July 28, 2022 at 13:34:49 (UTC).
See https://pubs.acs.org/sharingguidelines for options on how to legitimately share published articles.

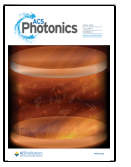
INTRODUCTION

Starting from the invention of the first light-emitting diodes (LEDs) in 1962,[1,2] today LEDs are widely used in various applications such as communications,[3] sensors,[4] automotive headlights,[5] transportation,[6] medicine,[7] backlighting in liquid-crystal displays (LCDs),[8] and general illumination.[9,10] In the near future, LEDs are expected to dominate lighting installations and have the potential to save 62 quads (quadrillion British thermal units) of energy by 2035.[11] Therefore, the impact of LED technology on energy will grow in the future.

For next-generation LED technologies, it is important to develop alternative and efficient solid-state lighting devices other than phosphors. These alternatives can enhance their functionality and meet the needs for the requirements of different applications. For that purpose, quantum dots (QDs) hold great promise because of their high efficiency and unique spectral tuning ability via the quantum confinement effect.[12−14] Recently, QDs have been started to be widely used by the TV industry, and the predictions show that QDs will further grow as an important building block for future display technology.[13] Even though color enhancement films made of QDs revolutionized the color quality of the TVs, one way to increase their potential use for a wide variety of application areas is to translate this unique nanomaterial into efficient LEDs. Toward that goal, nanorod formation for increasing the out-coupling coefficient[15] and silica mesoporous nanoparticle hybrids with QDs for spatial separation of emission and absorption[16] have been explored.

Alternatively, liquid-state integration allows for sensitive tuning of optical device characteristics by simple injection of QDs, enables suppression of the host-material effect, and keeps a high photoluminescence quantum yield (PLQY) of the QDs in the device architectures.[17−21] In addition to its benefits for

Received: November 25, 2021
Published: April 7, 2022



© 2022 The Authors. Published by American Chemical Society

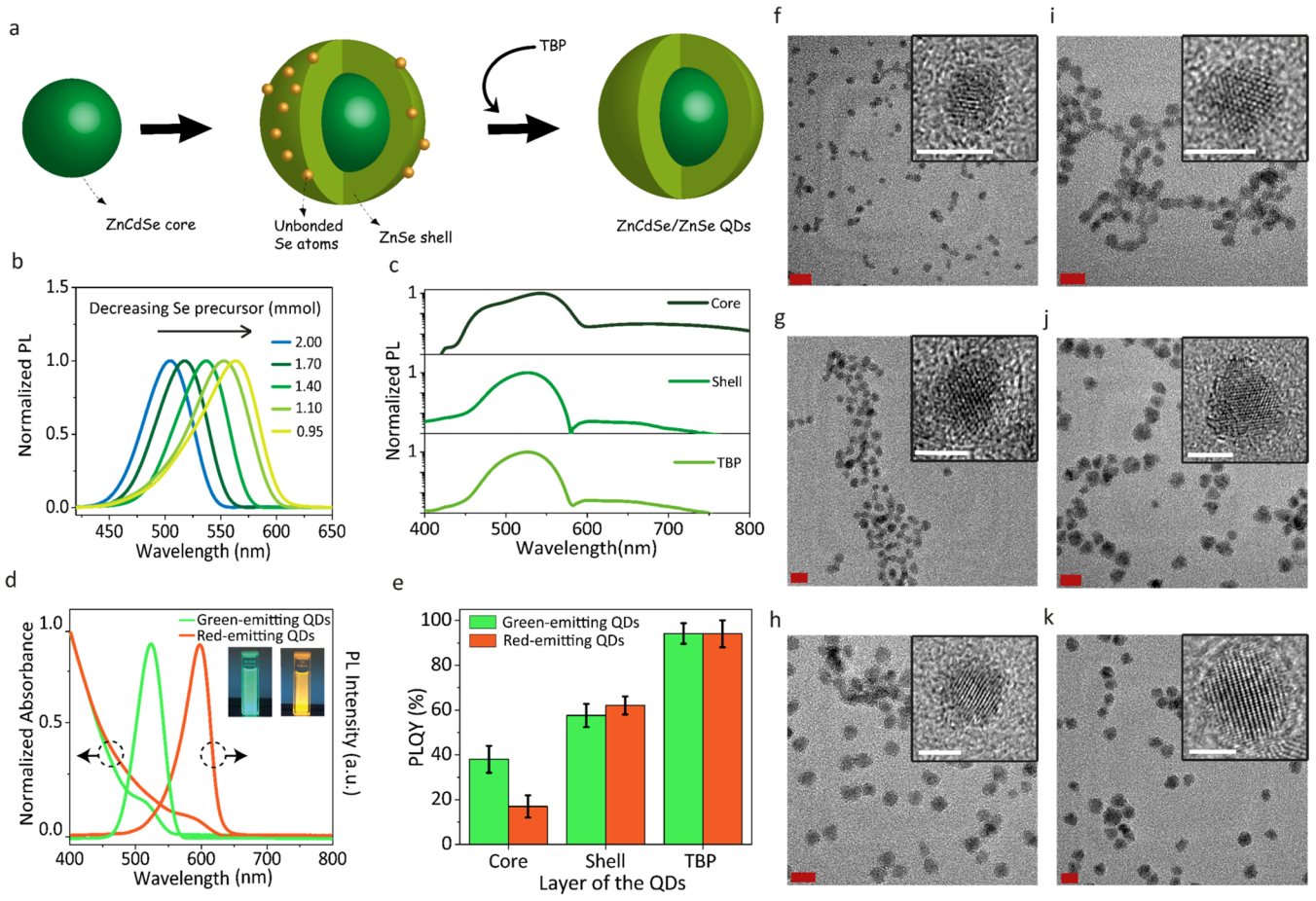


Figure 1. (a) Schematic of the synthesis procedure including ZnCdSe core formation, ZnSe shelling, and final TBP treatment. (b) Normalized PL spectra of ZnCdSe/ZnSe core/shell QDs at different injection amounts of the Se−SUS precursor ranging from 2.00 to 0.95 mmol of Se−SUS per 15 mL of solvent. (c) Normalized PL spectra of core, core/shell, and TBP-treated QDs. The surface trap state emission decreases after shelling and TBP treatment. (d) Normalized photoluminescence and absorbance spectra of green- and red-emitting ZnCdSe/ZnSe QDs after the TBP treatment, which are used for RGB-white LED. Inset: Photographs of TBP-treated green- and red-emitting ZnCdSe/ZnSe QDs under 365 nm UV irradiation. (e) Measured PLQY of the ZnCdSe core, ZnCdSe/ZnSe core/shell, and TBP-treated core/shell QDs (n = 3). Transmission electron microscopy (TEM) images of (f) green-emitting ZnCdSe core, (g) ZnCdSe/ZnSe core/shell, and (h) TBP-treated green-emitting ZnCdSe/ZnSe core/shell and (i) red-emitting ZnCdSe core, (j) ZnCdSe/ZnSe core/shell, and (k) TBP-treated red-emitting ZnCdSe/ZnSe core/shell QDs (red colored scale bar: 10 nm). The insets demonstrate the high-resolution transmission electron microscopy (HRTEM) images of (f, i) ZnCdSe core, (g, j) ZnCdSe/ZnSe core/shell, and (h, k) TBP-treated ZnCdSe/ZnSe core/shell for green- and red-emitting QDs, respectively (white colored scale bar: 5 nm).

efficiency, liquid-state integration can be advantageous in terms of thermal management of LEDs as well.[22,23] The investigation of the remote and liquid-state QD-LEDs showed that liquid can keep the temperature of the device as low as 50 °C, while in remote QD-LEDs, the temperature can elevate to 200 °C, especially at high injection currents.[23] Thus, the usage of QDs in a liquid form in the device architecture keeps the surface temperature low and enhances the device's reliability.[23] However, using this technique, the record efficiency of white LEDs (WLEDs) has remained around 100 lm/W.[18]

In this study, we demonstrate WLEDs over 150 lm/W using QDs in liquid. For that we sensitively optimized nucleation-growth conditions and obtained highly efficient green- and red-emitting ZnCdSe/ZnSe QDs with near-unity PLQY of 94.1 and 94.2% via postsynthesis removal of the surface traps, respectively. According to the optical simulations based on the radiative energy transfer, we integrated simulated amounts of green- and red-emitting QDs in a liquid state onto the blue LED chips, which led to red-green-blue (RGB)- and green-blue (GB)-based WLEDs with a maximum luminous efficiency of 129.6 and 170.4 lm/W, respectively. Hence, liquid-state integration of efficient nanomaterials holds promise for high-performance WLEDs.

RESULTS AND DISCUSSION

For WLEDs, ZnCdSe/ZnSe core/shell QDs were synthesized by low-temperature nucleation and high-temperature shell growth followed by tributylphosphine (TBP) treatment (Figure 1a).[24−26] Initially, we determined the proper composition of the ZnCdSe/ZnSe QDs that can emit within the green spectral range. The effective band gap of the green-emitting QDs can be controlled by varying the mole ratio of selenium (Se) that leads to a photoluminescence (PL) shift from 506 to 565 nm (Figure 1b) (see Figure S1). ZnCdSe QDs showing a peak emission wavelength at 543 nm were selected as the core. In addition to the radiative interband recombination, strong emission below the band-gap energy was also generated, which originated from the excess or unpassivated Cd/Zn surface sites on ZnCdSe QDs[26] that

https://doi.org/10.1021/acsphotonics.1c01805
ACS Photonics 2022, 9, 1304−1314

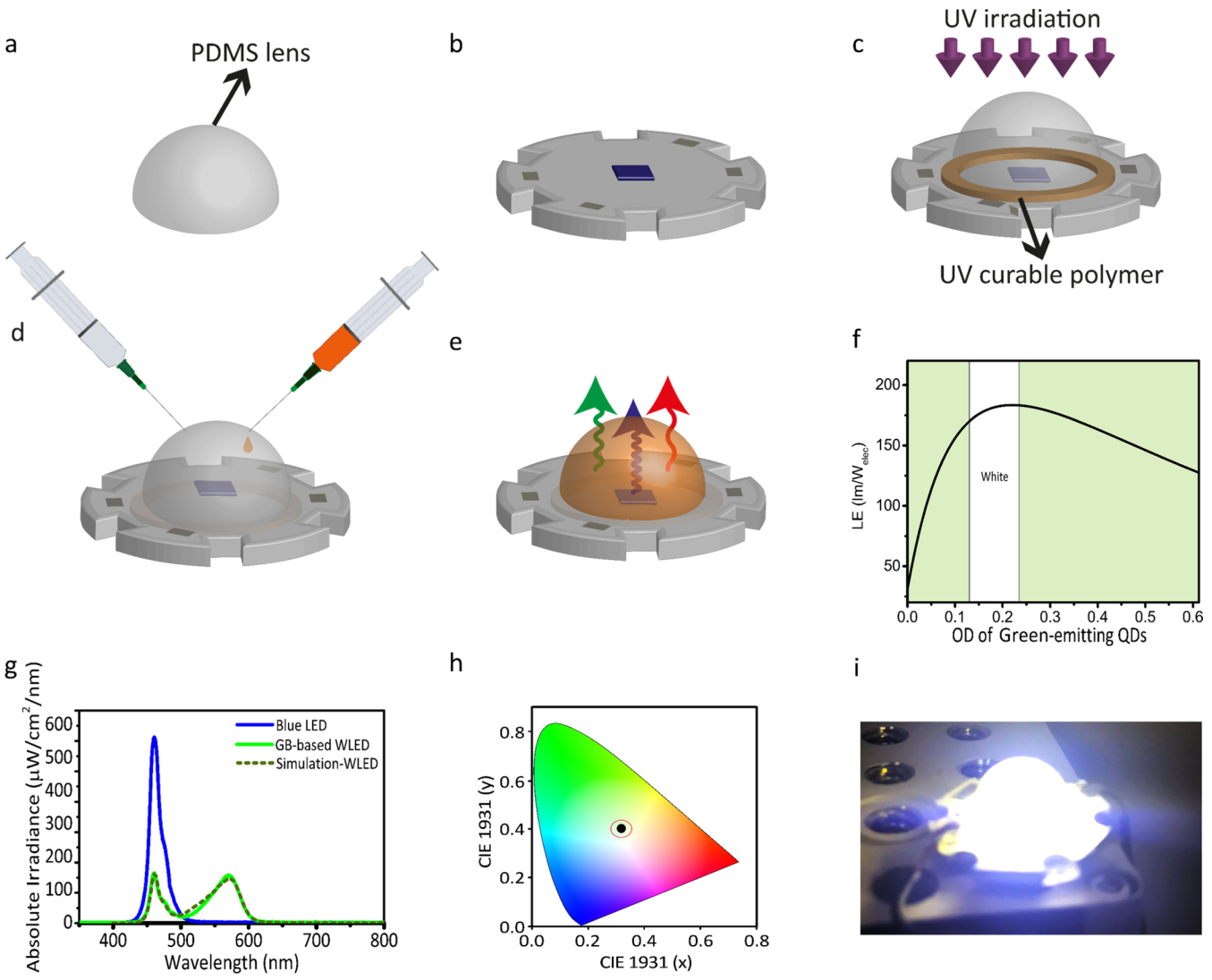


Figure 2. (a) Semispherical PDMS polymeric lens. (b) Blue LED chip soldered onto a printed circuit board (PCB) board. (c) PDMS lens was placed on top of the board, adhered to a UV curable polymer, and irradiated with a 365 nm UV lamp. (d) Red- and green-emitting QDs were injected into the lens by a syringe, while another syringe was used to evacuate the air inside of the lens. (e) White light generation as a combination of the blue electroluminescence from the LED and green and red emission from the QDs. (f) Simulation result of luminous efficiency of green-emitting QD-based WLED at different optical densities ranging from 0.13 to 0.23. The combinations corresponding to (x, y) chromacity color coordinates within the white region are shown. (g) Electroluminescence (EL) spectrum of the blue LED and GB-WLED at 5 mA injection current and the simulation via matrix formulation using radiative energy transfer (dashed line). (h) CIE 1931 color coordinate of the GB-WLED under a current injection level of 5 mA. (i) Photograph of WLED using QD liquids when it was turned on.

decrease the PLQY of the QDs. Hence, a PLQY of 38.2% was observed for only ZnCdSe core QDs (Figure 1e).

A ZnSe shell was selected due to the low lattice mismatch (about 2.4%)[27] between the core and shell materials, and it can form a type-I band alignment with the ZnCdSe core that can lead to the effective confinement of electron and hole wavefunctions mainly in the core region for efficient recombination of the photogenerated excitons. After the shell formation, the trap emission is significantly suppressed, which is also observed by the drop of the radiative defect state emission (Figure 1c), and thus PLQY increased to 57.6% (Figure 1e). Moreover, the PL peak showed a blue shift to 527 nm with respect to the core emission, which is due to the diffusion of the Zn and into the core during high-temperature shell growth,[28] which is in agreement with the shift observed on the peaks in the X-ray photoelectron spectrum of Zn 2p from 1021.93 and 1045.02 eV to 1017.46 and 1040.48 eV binding energies, respectively (Figures 1d and S4). In addition, the atomic percentage of cadmium (Cd) decreased from 2.66 to 0.29% (see Table S1 and Figure S4). Upon the growth of the ZnSe shell onto the ZnCdSe core QDs, diffraction patterns shifted to larger angles of 26.58, 44.62, and 52.38° with respect to the core corresponding to the (111), (220), and (311) planes of the zinc blende structure of ZnSe[29] that confirm the presence of the ZnSe shell (Figure S5). Moreover, the average particle size increases from 3.9 to 6.4 nm after the ZnSe shell growth, corresponding to a shell thickness of 1.2−1.3 nm (Figures 1f−h and S6).

Another factor affecting the efficiency of QDs is surface chemistry. Selenium dangling bonds can reduce the quantum yield of the QDs since they behave as the hole acceptor and introduce midgap states. We used TBP to passivate the surface defects.[28] The TBP amounts of 0.5, 1, 2, and 3 mL were injected into the ZnCdSe/ZnSe core/shell QD reaction flasks,

https://doi.org/10.1021/acsphotonics.1c01805
ACS Photonics 2022, 9, 1304−1314

and the PLQY was enhanced to 91.8, 92.6, 93.7, and 92.9%, respectively. In terms of the TBP amount, the injection of 2 mL achieved the highest PLQY under the same duration of 30 min at green PL (Figure S3a,b), and the TBP treatment of QDs does not significantly affect the emission wavelength (Figure S3b,c).[28,30,31] Furthermore, we also investigated the effect of TBP treatment time on PLQY. The PLQY of the QDs was gradually increased until 30 min of reaction time, and after 30 min, the PLQY remained almost constant, suggesting the saturation of removal of the unbonded anions on the QD surfaces. Finally, TBP treatment via passivation of Se^{2-} bonds led to a PLQY of 94.1% without the change of the emission peak (527 nm) and full-width at half maximum (FWHM) (46 nm) (Figure 1c). After TBP treatment, QDs did not also exhibit significant size variation (Figures 1h and S6). A similar structural optimization like the green-emitting QDs is done for red-emitting QDs, which led to a PLQY of 17% for the ZnCdSe core and increased to 62.1% with a zinc blende ZnSe shell (Figure 1e) (see Figure S2). Finally, TBP treatment led to red-emitting ZnCdSe/ZnSe QDs with a PLQY of 94.2% and emission at 601 nm with a mean particle size of 8.7 nm, suitable for efficient white light generation (Figures 1d,e,i−k and S6).

To demonstrate the surface passivation of the Se dangling bonds via TBP treatment, we performed proton-decoupled phosphorus nuclear magnetic resonance ($^{31}P\{^{1}H\}$-NMR) analysis on the QDs before and after the centrifugation processes. The existence of TBP ligands on QDs was readily proved by the $^{31}P\{^{1}H\}$-NMR analysis, which is a methodology that allowed us to clearly see the change in the chemical environment of phosphorus atoms in TBP. After the synthesis of QDs, the resulting crude mixture before the purification process was immediately analyzed by $^{31}P\{^{1}H\}$-NMR. As shown in $^{31}P\{^{1}H\}$-NMR spectra in Figure S7, the TBP−Se peak was observed at 36.27 ppm along with the peaks attributing the residual TBP and TBPO at −28.00 and 48.00 ppm, respectively. After the purification process, the $^{31}P\{^{1}H\}$-NMR spectrum revealed that the Se−P peak still remained at 36.27 ppm (Figure S7). Moreover, the residual phosphorus precursors were removed from the main QDs solution as byproducts. These results indicated that TBP molecules attached to the Se atoms on the surface of QDs, which is consistent with the literature as well.[32−34]

Various studies have demonstrated that ions on the surface of QDs promote distinct lifetime channels for electrons and holes of QDs. For example, cations induce long lifetime channels, whereas anions induce short lifetime channels.[28] We employed a time-correlated single-photon counting (TCSPC) system (MicroTime 100, Picoquant) to resolve their time-resolved photoluminescence (TRPL) characteristics. A nanosecond pulsed laser (λ = 375 nm) was used to pump QDs, and the PL decay was measured. Figure S3d shows the PLQYs and lifetimes for these QDs, where the average lifetime (τ_{avg}) was determined using an amplitude weighted mean as follows

$$\tau_{avg} = \frac{A_1\tau_1^2 + A_2\tau_2^2}{A_1\tau_1 + A_2\tau_2} \quad (1)$$

The PL decay curve of cation-rich ZnCdSe core QDs (owing to a high amount of Zn^{2+} ions) and ZnCdSe/ZnSe QDs can be fitted with one slow and one fast channel.[28] Excess cations on the surface of QDs possibly form shallow electron traps with a long lifetime. Due to the high intersolubility of TBP and Se, surface imperfections of excess Se^{2-} ions can be removed. Hence, the TBP treatment increased the PLQY of ZnCdSe/ZnSe QDs and changed their PL decay dynamics to an approximately monoexponential.

Because of the side effects of blue LEDs at 450 nm, there is a strong demand to shift the wavelength of the pumping LED toward the 460−475 nm spectral region.[35] The exposure of shorter blue wavelengths on the retinal pigment epithelium can danger photoreceptors via photochemical damage.[36,37] On the other side, emission wavelengths greater than 475 nm sacrifice color saturation and result in poor image quality. As a result, the lighting industry is moving toward the spectral window of 460−475 nm, and in this study, we employed blue LEDs with a wavelength of 460 nm.

To conserve PLQY of the QDs, we fabricated LEDs that can hold the QDs dissolved in toluene on top of the blue LED. The polydimethylsiloxane (PDMS) elastomer was selected as the polymeric lens material due to the high transparency in the visible region, flexibility, low cost, and large-scale fabrication ability.[18,38,39] The PDMS lens (Figure 2a), which is fabricated by curing in a mold, was adhered on top of the blue led chip (Figure 2b) by sealing its edges with UV curable polymer resin (Figure 2c). Once the UV curing process is finished, two micro syringes were used for green- and red-emitting QD solution injection: one syringe filled the lens with the QD solution, while the other syringe removed the trapped air (Figure 2d). PDMS can recover the puncture by the microsyringe because of its softness and hold the liquid on top of the blue LED chip without any leakage. The combination of the blue electroluminescence from the LED chip and the green and red PL from the excited QDs generate white light (Figure 2e,i).

To understand the proper range of injection amounts and the performance limits, we used a matrix formulation using the concept of radiative energy transfer because of its good agreement with the experimental measurements.[40] Briefly, the formulation encompasses all of the photonic processes in the color-conversion medium, which are absorption of the pump excitation and the resultant photoluminescence, self-absorption by the same-type fluorophores and photoluminescence due to the self-absorption, interabsorption due to a spectral overlap between the absorption of one type of fluorophore (*e.g.*, red-emitting QDs) and photoluminescence of the other types of fluorophores (*e.g.*, green-emitting QDs), and photoluminescence due to their interabsorption. For the calculation of the radiative energy transfer processes, the electroluminescence spectrum of the blue-emitting LED, absorption coefficient, spectral PL intensity, and PLQY of green- and red-emitting QDs are measured for the matrix formulation.

For a mixture of two types of QDs, it is important to identify the ratio of pump electroluminescence that is absorbed by each fluorophore. For that a homogeneous mixture of QDs is considered, and the κ factor is defined for each QD (eq 2), which represents the absorption ratio of the electroluminescent pump by the respective QD type (*e.g.*, green or red-emitting QDs). Next emission strength (W) for each QD is calculated using eq 3, where Q_i is the quantum yield of the fluorophore, $\alpha(\lambda)$ is the absorption coefficient of the fluorophores, D_j is the path length of the respective fluorophore, and $S_{in}(\lambda)$ is the power spectral density of the electroluminescent blue pump. To consider the overall interactions of quantum dots between each other, such as the reabsorption and interabsorption coefficient, $\bar{\bar{M}}$ describing reabsorption and interabsorption processes is introduced (eq 4). Diagonals of the matrix $\bar{\bar{M}}$

https://doi.org/10.1021/acsphotonics.1c01805
ACS Photonics 2022, 9, 1304−1314

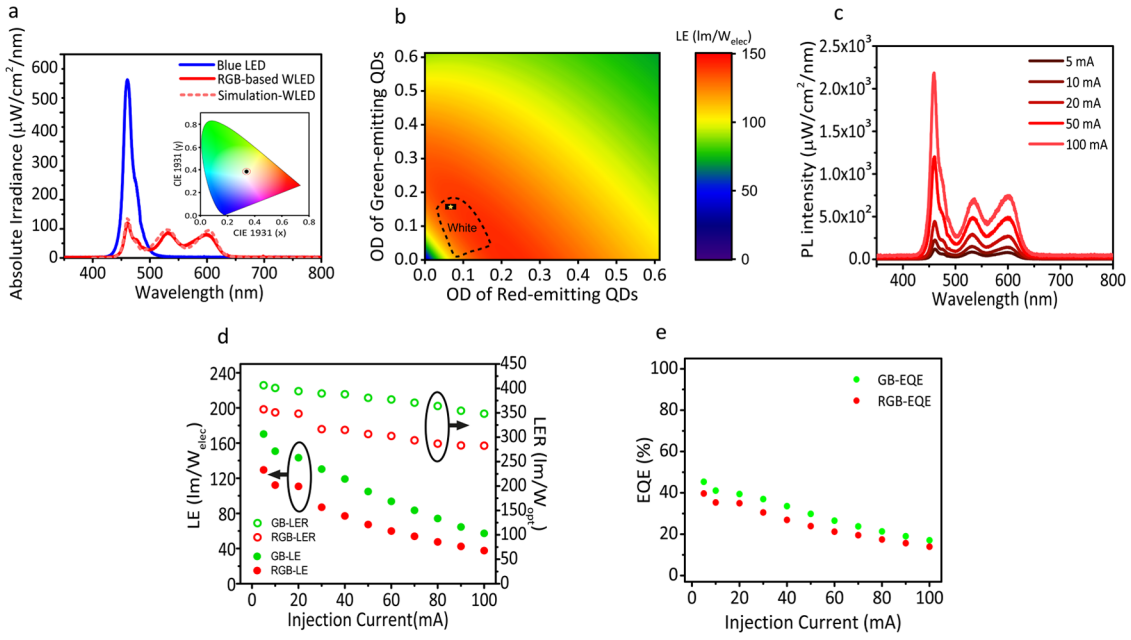


Figure 3. (a) Electroluminescence (EL) spectrum of the blue LED and RGB-WLED at the injection current level of 5 mA (inset: CIE 1931 color coordinate of the RGB-WLED). (b) Simulation of luminous efficiency of green- and red-emitting QD-based LED combinations at different optical density levels. The white region is exhibited with the black dashed line. The marked point is the experimental result of RGB-based WLEDs. (c) RGB-WLED spectra at different injection currents ranging from 5 to 100 mA. (d) Luminous efficiency (LE) and luminous efficacy of optical radiation (LER) of GB and RGB-WLEDs at different injection current levels. (e) External quantum efficiency (EQE) of GB and RGB-WLEDs at different injection current levels.

originate from reabsorption of the QDs and off-diagonal terms of matrix $\overline{\overline{M}}$ originate from interabsorption between QDs. $\overline{\overline{P}}$ (in eqs 5 to 6) is the normalized photoluminescence of the QDs with respect to area. $C\overline{\overline{P}}$ (in eq 7) is the sum of infinitely many cycles of reabsorption and interabsorption of red and green QDs (eqs 3−6). Finally, S_{out}, the power spectral density of the output spectrum, is calculated using eq 8. Notably, before using matrix formulation, all power spectral densities are converted into photon counts and then the output spectrum is calculated and converted back into power spectral density from photon counts. Since the quantum dots are at the nanoscale, the scattering factor is ignored. Over 1 million LED spectra were simulated using the optical properties of synthesized green- and red-emitting QDs, and the blue LED and their photometric properties such as luminous efficiency (i.e., lumen per electrical Watt), luminous efficacy of optical radiation (i.e., lumen per optical Watt), and (x, y) chromacity color coordinates were analyzed (see the Supporting Information).

$$\kappa_i(\lambda) = \frac{\alpha_i(\lambda)D_i}{\sum_j \alpha_j(\lambda)D_j} \tag{2}$$

$$W_i = Q_i \int S_{in}(\lambda)\kappa_i(\lambda)\left\{1 - \exp\left[-\sum_j \alpha_j(\lambda)D_j\right]\right\}d\lambda \tag{3}$$

$$M = \begin{pmatrix} M_{1,1} & \cdots & M_{1,j} \\ \vdots & \ddots & \vdots \\ M_{i,1} & \cdots & M_{1,j} \end{pmatrix} \tag{4}$$

$$M_{i,j} = Q_j \int P_i(\lambda)\kappa_j(\lambda)\left\{1 - \exp\left[-\sum_j \alpha_j(\lambda)D_j\right]\right\}d\lambda \tag{5}$$

$$P = \begin{pmatrix} P_{1,1} & \cdots & P_{1,n} \\ \vdots & \ddots & \vdots \\ P_{j,1} & \cdots & P_{j,n} \end{pmatrix} \tag{6}$$

$$\overline{\overline{C}} = (I - \overline{\overline{M}})^{-1} \exp\left[-\sum_j \alpha_j(\lambda)D_j\right] \tag{7}$$

$$\overrightarrow{S_{out}} = \overrightarrow{S_{in}} \exp\left[-\sum_j \alpha_j(\lambda)D_j\right] + \vec{W}^T \times \overline{\overline{C}} \times \overline{\overline{P}} \tag{8}$$

The simulation results for GB-WLEDs showed that green-emitting QDs with an OD range of 0.13−0.23 can lead to luminous efficiency levels above 166.6 lm/W (Figure 2f), which is achievable using blue LEDs with an external quantum efficiency of 65.8% (see Figure S8). Moreover, a maximum luminous efficiency of 184.0 lm/W can be obtained. According to the simulations, we injected green-emitting QDs with the OD of 0.155 into the lens (Figure 2g). The combination of green emission and blue light led to the (x, y) coordinates of (0.31, 0.40), which was within the white region,[41] and the emission corresponds to a white color with a cool daylight appearance with a correlated color temperature (CCT) at 6143 K (Figure 2h). Advantageously, the white LED showed a high luminous efficiency of 170.4 lm/W (see Table S3). Here, such high efficiency is achieved due to maintaining the QD efficiency levels within the device by liquid injection.

https://doi.org/10.1021/acsphotonics.1c01805
ACS Photonics 2022, 9, 1304−1314

For RGB-WLEDs, there exist a wide variety of green and red-emitting QD combinations for high-performance device operation (Figure 3b). According to the simulations, red- and green-emitting QDs having an optical density of 0.066 and 0.155 can lead to a maximum luminous efficiency of 141.4 lm/W with a color rendering index (CRI) value of 82 (Figure S9), respectively. We injected the simulated amounts of red- and green-emitting QDs on blue LED, and a luminous efficiency of 129.6 lm/W was observed (see Table S4). Moreover, the CRI of the WLED is 80, which corresponds to a sufficiently high level for lighting application to render the true colors of the illuminated objects (see Figure S10). The generated white light spectra based on RGB were in close agreement with the simulation spectra (Figure 3a). Our experimental results revealed that the CCTs of WLED and simulated results were also close to each other at 5417 K and 5446 K, respectively. The (x, y) chromacity color coordinates of RGB-WLED were (0.33, 0.38) within the white region (inset of Figure 3a). The RGB-WLED showed an external quantum efficiency of 39.6%, which is almost twice the previous WLED using QD liquids.[18] Moreover, we did a long-term optical stability test up to 1500 h (Figure S13). For that QDs in a glass lens were integrated into a blue LED to keep the liquid without any evaporation and interaction with the lens. The GB-WLED exhibited a good lifetime and T95 was 409 h. Using an exponential fit, the T75 and T50 lifetimes were extrapolated as 2325 h and 5602 h, respectively. In addition, the liquid helps to cool the LED chip and the lens broadens the illumination angle (Figure S12).

DISCUSSION

The previous luminous efficiency (LE) performance of color-conversion WLEDs is summarized in Figure 4. Some of the

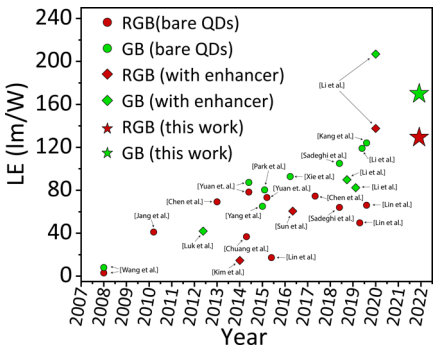


Figure 4. Luminous efficiency (LE) levels of previous white LEDs using QDs as the color converters. The star symbols are the efficiency levels achieved in this study.[8,16,18,42,44−61]

studies used only QDs as the color converters, and some of the studies added enhancers such as mesoporous silica particles to increase the device efficiency levels in addition to QDs. For WLEDs using only green-emitting QDs, the reported luminous efficiencies range from 65 to 125 lm/W. Here, one of the limiting factors was the efficiency of green QDs within the device architecture, which is here overcome by the simultaneous liquid-state injection and efficiency optimization. For white LEDs using both green- and red-emitting QDs, it is also important to incorporate red-emitting QDs with a peak emission wavelength corresponding to high values of eye sensitivity function for high luminous efficiency. In this study, this requirement is satisfied by purposely synthesizing red-emitting QDs having an emission peak below 620 nm. In future studies, the addition of red-emitting quantum dots above 620 nm can improve R9 for high-quality rendering of reddish colors.[42,43] Our device architecture and the luminous efficiency of high-PLQY QDs enabled high efficiency levels, getting closer to the LEDs using enhancers.[16] As a perspective, our simulation results showed that if the blue LED chip with an EQE level of 85% is used with the QDs in this study, luminous efficiency over 230 lm/W is achievable (Figure S11), which is comparable to the state-of-the-art efficiency levels achieved with phosphor-based white LEDs.

Color conversion is an industry-level applicable approach for future efficient solid-state lighting (SSL) technology, which proved its potential via phosphor that we currently use in our homes, offices, cars, etc. As an alternative to the phosphor, quantum dots show high promise due to their high level of emission tunability, low scattering due to their nanosize, and efficient luminescence. Their sensitive emission tunability via the quantum confinement effect and compositional control enables them to match with the eye sensitivity function. This can lead to bright LEDs that can be efficiently sensed by the human retina, which is proved by the efficient conversion of electrical Watt to the lumen in this study.

The direct injection of QDs into LED architecture offers a simple strategy for color-conversion LEDs. Previously, various methods have been investigated for the integration of QDs onto LEDs such as inkjet printing,[62] pulsed spray,[63] mist fabrication,[64] electrohydrodynamic-jet spray,[65] transfer printing,[66] and three-dimensional (3D) printing.[67] However, the nonradiative surface states in QD solid-state films cannot be perfectly passivated even with excess ligand treatments, which leads to a lower PLQY in solid-state integrated devices.[68] For example, excitons in QDs can cause Förster-type resonance energy transfer to nonradiative exciton states in neighboring QDs,[69−71] which can be suppressed by engineering the shell thickness and Auger recombination.[72] Alternatively, QDs in liquids keep their efficiency without any interaction with other QDs and efficiency-decreasing host matrix.

One of the limitations that we observe in this study is the efficiency of the white LEDs under higher current injection levels. The efficiency levels of liquid green QD-WLED were examined from 5 to 100 mA (Figure 3c), and the LE of the WLED dropped from 170.4 to 57.3 lm/W by increasing the current injection level (Figure 3d). Similarly, the LE of the RGB-WLED decreased from 129.6 to 37.67 lm/W (Figure 3d). According to our investigation, here, the 15−20% decrease originated from the reduction of the luminous efficiency of optical radiation. For example, for GB-WLED, it decreases from 406.3 to 348.2 lm/W and for RGB-WLED, it decreases from 357.3 to 282.7 lm/W, while the current injection level increases from 5 to 100 mA (Figure 3d). The major factor affecting the efficiency is the EQE decrease of the blue LED pump used in this study. Thus, the EQE of the GB-WLED and RGB-WLED dropped from 45.3 to 17.0% and from 39.6 to 13.9%, respectively, while the current injection level was increased to 100 mA (Figure 3e). Therefore, blue LEDs that operate with minimal efficiency drop at higher current injection levels can lead to efficient high-power LEDs using liquid nanomaterials.

Even though the investigation on Cd-based optoelectronic devices, in particular, is actively ongoing for proof-of-concept implementations in the academy,[16,73−82] another major limitation to the use of cadmium in industries is the toxic

https://doi.org/10.1021/acsphotonics.1c01805
ACS Photonics 2022, 9, 1304−1314

heavy metal content. According to EU RoHS regulations,[83−85] the cadmium content in the nanostructure needs to be less than 100 ppm. In our case, the total cadmium concentration for the GB-based WLED structure is less than 1 ppm according to the inductively coupled plasma-mass spectrometry (ICP-MS) measurement results (Table S2), which are within the limits allowed by EU. The transition toward green nanomaterials such as carbon dots[86,87] and fluorescent proteins[88,89] can provide better technology in terms of environmental sustainability.

Herein, we developed highly efficient QD-based white LEDs using green- and red-emitting ZnCdSe/ZnSe core/shell QDs. We optimized spectral and efficiency features of QDs by sensitively tuning the synthetic conditions via the precursor mole ratio, reaction time, emission wavelength, and post-synthetic treatment. The efficiency of QDs is maintained within the device via liquid-state injection. The injection of the simulated amounts led to an efficiency level as high as 170 lm/W. Therefore, white LEDs based on QD liquids hold high promise for future lighting applications.

MATERIALS AND METHODS

Chemicals. Cadmium oxide (CdO, powder, ≥99.99%), zinc oxide (ZnO Reagent Plus, powder, 99.90%), 1-octadecene (ODE, 90%), paraffin oil, oleic acid (OA, technical grade, 90%), selenium (Se, 99.99%, powder), tributylphosphine (TBP, 97%), toluene (anhydrous, 99.8%), and ethanol (for analysis) were purchased from Sigma Aldrich. These chemicals were used without further purification.

Preparation of a Cd Precursor for a ZnCdSe Core. A total of 1 mmol CdO, 3 mmol OA, and 9 mL of paraffin oil were mixed in a 50 mL three-neck flask and degassed at 120 °C for 1 h. Then, the mixture was heated to 190 °C under nitrogen flow. It was maintained at this temperature until a colorless clear solution was observed.

Preparation of a Zn Precursor. Overall, 30 mmol ZnO, 132 mmol OA, and 33 mL of paraffin oil were mixed in a 100 mL three-neck flask and degassed at 120 °C for 1 h. After that, the mixture was heated to 300 °C under nitrogen flow and kept for 1 h to achieve a transparent light-yellow solution.

Preparation of a Se Precursor for a ZnCdSe Core. A mixture of 4 mmol Se and 125 mmol ODE was degassed at 120 °C for 1 h in a 100 mL three-neck flask. Next, it was heated to 220 °C under nitrogen flow for 3 h, which led to a transparent yellowish solution.

Preparation of a 0.3 M Se-Octadecene Suspension (Se−SUS) Precursor for a ZnSe Shell. Overall, 9 mmol Se and 94 mmol ODE were mixed and degassed at 120 °C for 30 min in a 100 mL three-neck flask. Afterward, the mixture was heated to 240 °C under nitrogen flow for 30 min to obtain a yellow color solution.

Synthesis of Green-Emitting ZnCdSe/ZnSe Core/Shell QDs. A ZnCdSe core was synthesized based on the method by Li et al.[26] with modifications. A total of 10 mL of paraffin oil and a 0.5 mmol Se precursor solution were mixed in a 100 mL three-neck flask. The solution was heated to 150 °C in the presence of nitrogen gas. At this temperature, the solution was evacuated by vacuum for 50 min. After the degassing process, it was heated to 290 °C under an inert atmosphere. At this point, a 1.6 mmol Zn precursor was injected swiftly into the reaction flask and kept for long enough for the temperature to recover again. Afterward, a 0.1 mmol Cd precursor solution was swiftly injected into the flask. Right after, the temperature was set to 260 °C and held for 30 min.

ZnCdSe/ZnSe core/shell quantum dots were synthesized based on the method by Zhang et al.[28] with modifications. In the flask where the core was synthesized, the following processes were applied to form the shell on the core. The reaction flask was heated to 310 °C, at which a 0.6 mmol Se−SUS precursor solution was injected drop by drop into the flask at a rate of 12 mL/h using a syringe pump. After the injection was finished, the temperature was kept at 310 °C for 30 min for growing of the shell. Then, the solution was cooled to room temperature by removing the heating mantle. When the flask temperature reached room temperature, 2 mL of TBP was injected into the solution followed by stirring it for 30 min.

The QD synthesis solution was mixed with toluene and ethanol at a volume ratio of 1:4:2. Then, centrifugation was done at 9000 rpm for 10 min. Precipitated QDs were dispersed in toluene. Afterward, this solution was mixed with ethanol and precipitated at 9000 rpm for 10 min. The final product was redispersed with toluene.

Synthesis of Red-Emitting ZnCdSe/ZnSe Core/Shell QDs. To synthesize the ZnCdSe core, a similar synthetic procedure with green-emitting QDs was used with different amounts of paraffin oil and the Se precursor of 10 mL and 0.5 mmol, respectively. The flask that contains the paraffin oil and the Se precursor was heated to 150 °C under nitrogen flow. At 150 °C, the solution was degassed for 50 min. Then, the reaction flask was heated to 290 °C under nitrogen gas and a 1.6 mmol preprepared Zn precursor was swiftly injected into the medium. After the temperature was recovered itself, a 0.25 mmol Cd precursor was swiftly injected into the reaction flask and the reaction temperature was set at 260 °C. The reaction was allowed for 30 min at this temperature for nucleation and further growth of the QDs.

The solution was heated to 310 °C and a 0.6 mmol Se−SUS precursor solution was injected into the flask at a rate of 12 mL/h using a syringe pump. Then, the solution was kept at this temperature for 30 min to increase the shell thickness. Next, the solution was cooled to room temperature by removing the heating mantle. A total of 2 mL of TBP was injected into the cooled solution and stirred for 30 min. The above purification technique was applied for the isolation of QDs from the mixture.

Optical and Structural Characterizations. Powder X-ray diffraction (XRD) measurements of green- and red-emitting ZnCdSe/ZnSe QDs were carried out using a Rigaku Miniflex XRD $\lambda_{\mathrm{Cu\,K}\alpha}$ = 1.54 Å with a 5° min^{-1} scan rate. XRD samples were prepared by drop-casting QDs dissolved in toluene onto 1 cm × 1 cm silicon wafers and heated to 120 °C and kept at this temperature for 2 h to dry liquid QDs on the silicon wafers. An Edinburgh Instruments Spectrofluorometer FS5 with a 150 W xenon lamp and an excitation monochromator were used to test UV/visible absorption and the PL spectra of the QDs. The excitation wavelength was 375 nm. For absorbance and PL spectroscopy, regular quartz cuvettes were used. An integrating sphere module in FS5 was used to measure the absolute fluorescence quantum yield. The measurement module included a 150-mm-diameter integrating sphere that was inserted into the FS5 device for the measurement of quantum yields. For TEM and HRTEM measurements, samples were deposited as 10 μL of a 1 mM QD in a hexane solution on a copper support grid. TEM and HRTEM analyses were performed using a JEOL JEM-

https://doi.org/10.1021/acsphotonics.1c01805
ACS Photonics 2022, 9, 1304−1314

ARM200CFEG UHR microscope with a spherical aberration-corrected probe and equipped with a Gatan UltraScan camera model 994 US1000X. A PicoQuant MicroTime 100 time-resolved confocal fluorescence microscope was used to detect time-dependent PL decays. A picosecond diode laser (λ_{exc} = 375 nm) at a 60 MHz repetition rate coupled to a 40× objective lens was used as an excitation beam. Bandpass filters with a bandwidth of 15 nm were utilized for spectrally resolved data. X-ray photoelectron spectroscopy (XPS) measurements were performed using a Thermo Scientific K-α (Al Kα source) surface analysis tool at ultrahigh vacuum conditions. XPS samples were prepared with the same technique as XRD sample preparation. The contents of the materials in the ZnCdSe/ZnSe core/shell QDs were determined using an Agilent 7700× inductively coupled plasma-mass spectrometer (ICP-MS). For the ICP-MS analysis, the powder samples were digested in 10 mL of aqua regia (8 mL HNO_3 + 2 mL HCl) via a Start D Milestone Microwave Digestion system and diluted with a 2 v/v % HNO_3 blank solution. Nuclear magnetic resonance (NMR) spectra were recorded on a Varian (operating at 500 MHz for ^{1}H NMR and 242 MHz for ^{31}P NMR) in $CDCl_3$ with tetramethylsilane (TMS) as an internal standard, and chemical shifts are given in parts per million (ppm). For ^{31}P {^{1}H} NMR experiments, the spectra of samples were collected using 8192 scans and the spectra were processed with the Bruker TopSpin 4.1.0 program.

Process for Producing Lenses. Overall, 1 g of a polydimethylsiloxane (PDMS) SYLGARD 184 elastomer was combined with 0.1 g of a SYLGARD 184 curing agent and vigorously stirred for 2 min till bubbles appeared in the mixture to make the semispherical lens. The mixture was then degassed for 30 min in a Bel-Art Space Saver Vacuum Desiccator before all bubbles were gone. To complete the PDMS curing process, the mixture was poured into a prefabricated aluminum mold and heated in an oven at 80 °C for 5 h. The aluminum mold was opened, and the lens was taken out after the heating was done. A semispherical lens with an outer diameter of 9 mm, an inner diameter of 7 mm, and a lens thickness of 1 mm was obtained.

Fabrication of an LED. A blue LED chip (Fujian Lightning Optoelectronic Co. Ltd.) was placed on a star-shaped aluminum printed circuit board (PCB), and two electrical wires were soldered to the board for connection to the voltage supply. Then, the PDMS lens was connected to the PCB with an NOA 68 UV curable optical adhesive for the curing process. In this process, the UV curable adhesive was added to the sides of the lens, and then it was cured for 1 h under UV irradiation at 365 nm. It was checked whether there was any place on the edges of the PDMS lens without adhesive. If there is a place where no adhesive has been added, more adhesive is added to prevent leakage of the lens if required.

LED Measurements. Ocean Optics integrating spheres were used for LED characterizations. An Ocean Optics Torus was used as a detector with a wavelength range of 300 to 900 nm with an optical resolution of 1.6 nm FWHM over the spectra range. An Ocean Insight HL-3P-INT-CAL was used as a calibration source. The luminescence efficiency calculation was performed according to ref 2.

CRI Calculation. CRI (Ra) was calculated by taking the average of R1−R8 values. For CRI calculation, we used the software tool OSRAM LED ColorCalculator.

■ ASSOCIATED CONTENT

Supporting Information

The Supporting Information is available free of charge at https://pubs.acs.org/doi/10.1021/acsphotonics.1c01805.

Absorption and photoluminescence spectrum, PLQY, time-resolved spectroscopy, XPS and XRD results, and size distribution analysis of synthesized and optimized core, core/shell, and TBP-treated ZnCdSe/ZnSe QDs; 31P {^{1}H} NMR analysis of the TBP-treated QDs with and without centrifugation; EQE, LE, and EL spectra of the blue LED at various current injections; simulation and experimental results of red- and green-emitting QDs based on CRI; simulation of GB-WLED in terms of LE by the usage of highly efficient blue LEDs; IR images of the surface temperature of LEDs with and without QDs; emission characteristics at different angles; operational lifetime test; ICP-MS measurements of ZnCdSe/ZnSe core/shell QDs; and optoelectronic performances of GB- and RGB-based WLEDs at various current injection levels (PDF)

■ AUTHOR INFORMATION

Corresponding Author

Sedat Nizamoglu − *Graduate School of Material Science and Engineering, Koç University, Istanbul 34450, Turkey; Graduate School of Biomedical Science and Engineering, Department of Electrical and Electronics Engineering, and Koc University Boron and Advanced Materials Application and Research Center, Koç University, Istanbul 34450, Turkey;* orcid.org/0000-0003-0394-5790; Email: snizamoglu@ku.edu.tr

Authors

Asim Onal − *Graduate School of Material Science and Engineering, Koç University, Istanbul 34450, Turkey;* orcid.org/0000-0003-3682-6042

Guncem Ozgun Eren − *Graduate School of Biomedical Science and Engineering, Koç University, Istanbul 34450, Turkey;* orcid.org/0000-0002-9297-9898

Sadra Sadeghi − *Graduate School of Material Science and Engineering, Koç University, Istanbul 34450, Turkey; Department of Electrical and Electronics Engineering, Koç University, Istanbul 34450, Turkey;* orcid.org/0000-0002-8569-1626

Rustamzhon Melikov − *Department of Electrical and Electronics Engineering, Koç University, Istanbul 34450, Turkey;* Present Address: Plasmon Nanotechnologies, Istituto Italiano di Tecnologia, 16163 Genova, Italy; orcid.org/0000-0003-2214-7604

Mertcan Han − *Department of Electrical and Electronics Engineering, Koç University, Istanbul 34450, Turkey;* orcid.org/0000-0002-3543-5894

Onuralp Karatum − *Department of Electrical and Electronics Engineering, Koç University, Istanbul 34450, Turkey;* orcid.org/0000-0002-7669-9589

Melek Sermin Ozer − *Department of Chemistry, Koç University, 34450 Istanbul, Turkey*

Houman Bahmani Jalali − *Graduate School of Biomedical Science and Engineering, Koç University, Istanbul 34450, Turkey;* Present Address: Photonic Nanomaterials, Istituto Italiano di Tecnologia, 16163 Genova, Italy; orcid.org/0000-0001-7212-9098

https://doi.org/10.1021/acsphotonics.1c01805
ACS Photonics 2022, 9, 1304−1314

Itir Bakis Dogru-Yuksel − *Graduate School of Biomedical Science and Engineering, Koç University, Istanbul 34450, Turkey;* orcid.org/0000-0001-8569-7625

Iskender Yilgor − *Department of Chemistry and Koç University Surface Science and Technology Center (KUYTAM), Koç University, 34450 Istanbul, Turkey;* orcid.org/0000-0002-7756-4192

Önder Metin − *Department of Chemistry, Koç University Surface Science and Technology Center (KUYTAM), and Koç University TÜPRAŞ Energy Center (KUTEM), Koç University, 34450 Istanbul, Turkey;* orcid.org/0000-0003-1622-4992

Complete contact information is available at: https://pubs.acs.org/10.1021/acsphotonics.1c01805

Funding

This work was financially supported by the Technological Research Council of Turkey (TUBITAK) with Project No. 115E115.

Notes

The authors declare no competing financial interest.

The data sets that support all of the findings of this study are available from the corresponding authors upon reasonable request.

■ ACKNOWLEDGMENTS

S.N. acknowledges the Scientific and Technological Research Council of Turkey (TUBITAK) with Project No. 115E115. S.N. acknowledges the support from the Turkish Academy of Sciences (TÜBA-GEBIP; The Young Scientist Award Program), the Science Academy of Turkey (BAGEP; The Young Scientist Award Program), and Bilim Kahramanları Derneği (The Young Scientist Award Program). The authors thank KUBAM (Koç University Boron and Advanced Materials Application and Research Center) for XRD and KUYTAM (Koç University Surface Science and Technology Center) for ICP. The authors also acknowledge UNAM (National Nanotechnology Research Center) for sincere efforts for TEM and XPS measurement.

■ REFERENCES

(1) Holonyak, N.; Bevacqua, S. F. COHERENT (VISIBLE) LIGHT EMISSION FROM $Ga(As_{1-x}P_x)$ JUNCTIONS. *Appl. Phys. Lett.* **1962**, *1*, 82−83.

(2) Schubert, E. F. *Light-Emitting Diodes*; Cambridge University Press, 2006.

(3) Minotto, A.; Haigh, P. A.; Łukasiewicz, G.; Lunedei, E.; Gryko, D. T.; Darwazeh, I.; Cacialli, F. Visible Light Communication with Efficient Far-Red/near-Infrared Polymer Light-Emitting Diodes. *Light Sci. Appl.* **2020**, *9*, No. 70.

(4) Ivanisevic, A.; Yeh, J. Y.; Mawst, L.; Kuech, T. F.; Ellis, A. B. Light-Emitting Diodes as Chemical Sensors. *Nature* **2001**, *409*, 476.

(5) Pust, P.; Schmidt, P. J.; Schnick, W. A Revolution in Lighting. *Nat. Mater.* **2015**, *14*, 454−458.

(6) Schubert, E. F.; Kim, J. K. Solid-State Light Sources Getting Smart. *Science* **2005**, *308*, 1274−1278.

(7) Lee, G. H.; Moon, H.; Kim, H.; Lee, G. H.; Kwon, W.; Yoo, S.; Myung, D.; Yun, S. H.; Bao, Z.; Hahn, S. K. Multifunctional Materials for Implantable and Wearable Photonic Healthcare Devices. *Nat. Rev. Mater.* **2020**, *5*, 149−165.

(8) Chen, H. W.; Zhu, R. D.; He, J.; Duan, W.; Hu, W.; Lu, Y. Q.; Li, M. C.; Lee, S. L.; Dong, Y. J.; Wu, S. T. Going beyond the Limit of an LCD's Color Gamut. *Light Sci. Appl.* **2017**, *6*, e17043−10.

(9) Nizamoglu, S.; Ozel, T.; Sari, E.; Demir, H. V. White Light Generation Using CdSe/ZnS Core-Shell Nanocrystals Hybridized with InGaN/GaN Light Emitting Diodes. *Nanotechnology* **2007**, *18*, 065709.

(10) Matioli, E.; Brinkley, S.; Kelchner, K. M.; Hu, Y. L.; Nakamura, S.; DenBaars, S.; Speck, J.; Weisbuch, C. High-Brightness Polarized Light-Emitting Diodes. *Light Sci. Appl.* **2012**, *1*, e22.

(11) Elliott, C.; Yamada, M.; Penning, J.; Schober, S.; Lee, K. *Energy Savings Forecast of Solid-State Lighting in General Illumination Applications*; Navigant Consulting: United States, 2019 DOI: 10.2172/1607661.

(12) Kagan, C. R.; Lifshitz, E.; Sargent, E. H.; Talapin, D. V. Building Devices from Colloidal Quantum Dots. *Science* **2016**, *353*, 885.

(13) Erdem, T.; Nizamoglu, S.; Demir, H. V. Computational Study of Power Conversion and Luminous Efficiency Performance for Semiconductor Quantum Dot Nanophosphors on Light-Emitting Diodes. *Opt. Express* **2012**, *20*, 3275.

(14) Jalali, H. B.; Sadeghi, S.; Dogru Yuksel, I. B.; Onal, A.; Nizamoglu, S. Past, Present and Future of Indium Phosphide Quantum Dots. *Nano Res.* **2022**, 1−22, DOI: 10.1007/s12274-021-4038-z.

(15) Prodanov, M. F.; Gupta, S. K.; Kang, C.; Diakov, M. Y.; Vashchenko, V. V.; Srivastava, A. K. Thermally Stable Quantum Rods, Covering Full Visible Range for Display and Lighting Application. *Small* **2021**, *17*, 2004487.

(16) Li, J. S.; Tang, Y.; Li, Z. T.; Li, J. X.; Ding, X. R.; Yu, B. H.; Yu, S. D.; Ou, J. Z.; Kuo, H. C. Toward 200 Lumens per Watt of Quantum-Dot White-Light-Emitting Diodes by Reducing Reabsorption Loss. *ACS Nano* **2021**, *15*, 550−562.

(17) Sadeghi, S.; Khabbaz Abkenar, S.; Ow-Yang, C. W.; Nizamoglu, S. Efficient White LEDs Using Liquid-State Magic-Sized CdSe Quantum Dots. *Sci. Rep.* **2019**, *9*, No. 10061.

(18) Sadeghi, S.; Kumar, B. G.; Melikov, R.; Aria, M. M.; Jalali, H. B.; Nizamoglu, S. Quantum Dot White LEDs with High Luminous Efficiency. *Optica* **2018**, *5*, 793−802.

(19) Li, J.-S.; Tang, Y.; Li, Z.-T.; Rao, L.-S.; Ding, X.-R.; Yu, B.-H. High Efficiency Solid−Liquid Hybrid-State Quantum Dot Light-Emitting Diodes. *Photonics Res.* **2018**, *6*, 1107−1115.

(20) Peter, E.; Subash, T. D. Synthesis of Red-Emitting CdSe/CdS/ZnS Core/Shell/Shell Quantum Dots. *Mater. Today Proc.* **2020**, *24*, 2144−2148.

(21) Eren, G. O.; Sadeghi, S.; Bahmani Jalali, H.; Ritter, M.; Han, M.; Baylam, I.; Melikov, R.; Onal, A.; Oz, F.; Sahin, M.; Ow-Yang, C. W.; Sennaroglu, A.; Lechner, R. T.; Nizamoglu, S. Cadmium-Free and Efficient Type-II InP/ZnO/ZnS Quantum Dots and Their Application for LEDs. *ACS Appl. Mater. Interfaces* **2021**, *13*, 32022−32030.

(22) Bar-Cohen, A.; Arik, M.; Ohadi, M. Direct Liquid Cooling of High Flux Micro and Nano Electronic Components. *Proc. IEEE* **2006**, *94*, 1549−1570.

(23) Sher, C.-W.; Lin, C.-H.; Lin, H.-Y.; Lin, C.-C.; Huang, C.-H.; Chen, K.-J.; Li, J.-R.; Wang, K.-Y.; Tu, H.-H.; Fu, C.-C.; Kuo, H. C. A High Quality Liquid-Type Quantum Dot White Light-Emitting Diode. *Nanoscale* **2016**, *8*, 1117−1122.

(24) Shen, H.; Bai, X.; Wang, A.; Wang, H.; Qian, L.; Yang, Y.; Titov, A.; Hyvonen, J.; Zheng, Y.; Li, L. S. High-Efficient Deep-Blue Light-Emitting Diodes by Using High Quality ZnxCd1-XS/ZnS Core/Shell Quantum Dots. *Adv. Funct. Mater.* **2014**, *24*, 2367−2373.

(25) Wang, A.; Shen, H.; Zang, S.; Lin, Q.; Wang, H.; Qian, L.; Niu, J.; Li, L. S. Bright, Efficient, and Color-Stable Violet ZnSe-Based Quantum Dot Light-Emitting Diodes. *Nanoscale* **2015**, *7*, 2951−2959.

(26) Li, Z.; Chen, F.; Wang, L.; Shen, H.; Guo, L.; Kuang, Y.; Wang, H.; Li, N.; Li, L. S. Synthesis and Evaluation of Ideal Core/Shell Quantum Dots with Precisely Controlled Shell Growth: Nonblinking, Single Photoluminescence Decay Channel, and Suppressed FRET. *Chem. Mater.* **2018**, *30*, 3668−3676.

(27) Jen, J. Y.; Lin, C. Y.; Lee, J. R.; Lu, C. R. Photoluminescence Characterization of ZnCdSe/ZnSe Quantum Dot Systems with

Different ZnCdSe Coverages. *J. Phys. Chem. Solids* **2008**, *69*, 485−489.
(28) Zhang, T.; Zhang, X.; Yang, P.; Bai, J.; Chang, C.; Jin, X.; Zhao, F.; Huang, Y.; Li, F. Bright Alloy CdZnSe/ZnSe QDs with Nonquenching Photoluminescence at High Temperature and Their Application to Light-Emitting Diodes. *J. Nanomater.* **2019**, *2019*, 1−8.
(29) Senthilkumar, K.; Kalaivani, T.; Kanagesan, S.; Balasubramanin, V. Synthesis and Characterization Studies of ZnSe Quantum Dots. *J. Mater. Sci.: Mater. Electron.* **2012**, *23*, 2048−2052.
(30) Hoisang, W.; Uematsu, T.; Torimoto, T.; Kuwabata, S. Luminescent Quaternary Ag(InxGa1- x)S2/GaSyCore/Shell Quantum Dots Prepared Using Dithiocarbamate Compounds and Photoluminescence Recovery via Post Treatment. *Inorg. Chem.* **2021**, *60*, 13101−13109.
(31) Pu, C.; Peng, X. To Battle Surface Traps on CdSe/CdS Core/Shell Nanocrystals: Shell Isolation versus Surface Treatment. *J. Am. Chem. Soc.* **2016**, *138*, 8134−8142.
(32) Jasieniak, J.; Mulvaney, P. From Cd-Rich to Se-Rich - The Manipulation of CdSe Nanocrystal Surface Stoichiometry. *J. Am. Chem. Soc.* **2007**, *129*, 2841−2848.
(33) Evans, C. M.; Evans, M. E.; Krauss, T. D. Mysteries of TOPSe Revealed: Insights into Quantum Dot Nucleation. *J. Am. Chem. Soc.* **2010**, *132*, 10973−10975.
(34) Liu, H.; Owen, J. S.; Alivisatos, A. P. Mechanistic Study of Precursor Evolution in Colloidal Group II-VI Semiconductor Nanocrystal Synthesis. *J. Am. Chem. Soc.* **2007**, *129*, 305−312.
(35) Prodanov, M. F.; Vashchenko, V. V.; Srivastava, A. K. Progress toward Blue-Emitting (460−475 Nm) Nanomaterials in Display Applications. *Nanophotonics* **2021**, *10*, 1801−1836.
(36) Tosini, G.; Bertolucci, C.; Foà, A. The Circadian System of Reptiles: A Multioscillatory and Multiphotoreceptive System. *Physiol. Behav.* **2001**, *72*, 461−471.
(37) Marek, V.; Potey, A.; Réaux-Le-Goazigo, A.; Reboussin, E.; Charbonnier, A.; Villette, T.; Baudouin, C.; Rostène, W.; Denoyer, A.; Mélik Parsadaniantz, S. Blue Light Exposure in Vitro Causes Toxicity to Trigeminal Neurons and Glia through Increased Superoxide and Hydrogen Peroxide Generation. *Free Radical Biol. Med.* **2019**, *131*, 27−39.
(38) Kumar, B. G.; Sadeghi, S.; Melikov, R.; Aria, M. M.; Jalali, H. B.; Ow-Yang, C. W.; Nizamoglu, S. Structural Control of InP/ZnS Core/Shell Quantum Dots Enables High-Quality White LEDs. *Nanotechnology* **2018**, *29*, No. 345605.
(39) Sadeghi, S.; Melikov, R.; Bahmani Jalali, H.; Nizamoglu, S. Ultraefficient Green LEDs Using Quantum Dots in Liquid Matrix. *IEEE Trans. Electron Devices* **2019**, *66*, 4784−4789.
(40) Melikov, R.; Press, D. A.; Ganesh Kumar, B.; Sadeghi, S.; Nizamoglu, S. Unravelling Radiative Energy Transfer in Solid-State Lighting. *J. Appl. Phys.* **2018**, *123*, 23103.
(41) Erdem, T.; Nizamoglu, S.; Sun, X. W.; Demir, H. V. A Photometric Investigation of Ultra-Efficient LEDs with High Color Rendering Index and High Luminous Efficacy Employing Nanocrystal Quantum Dot Luminophores. *Opt. Express* **2010**, *18*, 340.
(42) Yuan, X.; Hua, J.; Zeng, R.; Zhu, D.; Ji, W.; Jing, P.; Meng, X.; Zhao, J.; Li, H. Efficient White Light Emitting Diodes Based on Cu-Doped ZnInS/ZnS Core/Shell Quantum Dots. *Nanotechnology* **2014**, *25*, 435202.
(43) Yang, W.; Zhong, P.; Mei, S.; Chen, Q.; Zhang, W.; Zhu, J.; Guo, R.; He, G. Photometric Optimization of Color Temperature Tunable Quantum Dots Converted White LEDs for Excellent Color Rendition. *IEEE Photonics J.* **2016**, *8*, 1−11.
(44) Yang, S. J.; Oh, J. H.; Kim, S.; Yang, H.; Do, Y. R. Realization of InP/ZnS Quantum Dots for Green, Amber and Red down-Converted LEDs and Their Color-Tunable, Four-Package White LEDs. *J. Mater. Chem. C* **2015**, *3*, 3582−3591.
(45) Park, S. H.; Hong, A.; Kim, J. H.; Yang, H.; Lee, K.; Jang, H. S. Highly Bright Yellow-Green-Emitting CuInS2 Colloidal Quantum Dots with Core/Shell/Shell Architecture for White Light-Emitting Diodes. *ACS Appl. Mater. Interfaces* **2015**, *7*, 6764−6771.
(46) Yuan, X.; Ma, R.; Zhang, W.; Hua, J.; Meng, X.; Zhong, X.; Zhang, J.; Zhao, J.; Li, H. Dual Emissive Manganese and Copper Co-Doped Zn-In-S Quantum Dots as a Single Color-Converter for High Color Rendering White-Light-Emitting Diodes. *ACS Appl. Mater. Interfaces* **2015**, *7*, 8659−8666.
(47) Lin, H. Y.; Wang, S. W.; Lin, C. C.; Chen, K. J.; Han, H. V.; Tu, Z. Y.; Tu, H. H.; Chen, T. M.; Shih, M. H.; Lee, P. T.; Chen, H. M. P.; Kuo, H. C. Excellent Color Quality of White-Light-Emitting Diodes by Embedding Quantum Dots in Polymers Material. *IEEE J. Sel. Top. Quantum Electron.* **2016**, *22*, 35−41.
(48) Sun, C.; Zhang, Y.; Ruan, C.; Yin, C.; Wang, X.; Wang, Y.; Yu, W. W. Efficient and Stable White LEDs with Silica-Coated Inorganic Perovskite Quantum Dots. *Adv. Mater.* **2016**, *28*, 10088−10094.
(49) Xie, B.; Hu, R.; Yu, X.; Shang, B.; Ma, Y.; Luo, X. Effect of Packaging Method on Performance of Light-Emitting Diodes with Quantum Dot Phosphor. *IEEE Photonics Technol. Lett.* **2016**, *28*, 1115−1118.
(50) Li, J.-S.; Tang, Y.; Li, Z.-T.; Rao, L.-S.; Ding, X.-R.; Yu, B.-H.; et al. High Efficiency Solid − Liquid Hybrid-State Quantum Dot Light-Emitting Diodes. *Photonics Res.* **2018**, *6*, 1107−1115.
(51) Li, J.; Tang, Y.; Li, Z.; Ding, X.; Yu, B.; Lin, L. Largely Enhancing Luminous Efficacy, Color-Conversion Efficiency, and Stability for Quantum-Dot White LEDs Using the Two-Dimensional Hexagonal Pore Structure of SBA-15 Mesoporous Particles. *ACS Appl. Mater. Interfaces* **2019**, *11*, 18808−18816.
(52) Li, Z. T.; Li, J. X.; Li, J. S.; Du, X. W.; Song, C. J.; Tang, Y. Thermal Impact of LED Chips on Quantum Dots in Remote-Chip and On-Chip Packaging Structures. *IEEE Trans. Electron Devices* **2019**, *66*, 4817−4822.
(53) Kang, C. Y.; Lin, C. H.; Lin, C. H.; Li, T. Y.; Huang Chen, S. W.; Tsai, C. L.; Sher, C. W.; Wu, T. Z.; Lee, P. T.; Xu, X.; Zhang, M.; Ho, C. H.; He, J. H.; Kuo, H. C. Highly Efficient and Stable White Light-Emitting Diodes Using Perovskite Quantum Dot Paper. *Adv. Sci.* **2019**, *6*, 1902230.
(54) Lin, C.-H.; Verma, A.; Kang, C.-Y.; Pai, Y.-M.; Chen, T.-Y.; Yang, J.-J.; Sher, C.-W.; Yang, Y.-Z.; Lee, P.-T.; Lin, C.-C.; Wu, Y.-C.; Sharma, S. K.; Wu, T.; Chung, S.-R.; Kuo, H.-C. Hybrid-Type White LEDs Based on Inorganic Halide Perovskite QDs: Candidates for Wide Color Gamut Display Backlights. *Photonics Res.* **2019**, *7*, 579.
(55) Lin, C.-H.; Kang, C.; Verma, A.; Wu, T.; Pai, Y.; Lee, P.; Chung, S.; Kuo, H.; et al.*et al.* Ultrawide Color Gamut Perovskite and CdSe / ZnS Quantum-Dots-Based White Light-Emitting Diode with High Luminous Efficiency. *Nanomaterials* **2019**, *9*, 1314.
(56) Wang, H.; Lee, K. S.; Ryu, J. H.; Hong, C. H.; Cho, Y. H. White Light Emitting Diodes Realized by Using an Active Packaging Method with CdSe/ZnS Quantum Dots Dispersed in Photosensitive Epoxy Resins. *Nanotechnology* **2008**, *19*, 145202.
(57) Jang, B. E.; Jun, S.; Jang, H.; Lim, J.; Kim, B.; Kim, Y. White-Light-Emitting Diodes with Quantum Dot Color Converters for Display Backlights. *Adv. Mater.* **2010**, *22*, 3076−3080.
(58) Luk, C. M.; Tang, L. B.; Zhang, W. F.; Yu, S. F.; Teng, K. S.; Lau, S. P. An Efficient and Stable Fluorescent Graphene Quantum Dot-Agar Composite as a Converting Material in White Light Emitting Diodes. *J. Mater. Chem.* **2012**, *22*, 22378−22381.
(59) Chen, B.; Zhong, H.; Wang, M.; Liu, R.; Zou, B. Integration of CuInS2-Based Nanocrystals for High Efficiency and High Colour Rendering White Light-Emitting Diodes. *Nanoscale* **2013**, *5*, 3514−3519.
(60) Kim, Y. K.; Choi, K. C.; Baek, Y. K.; Shin, P. W. Enhanced Luminescence Stability of Quantum Dot-Based Inorganic Nanocomposite Particles for White-Light-Emitting Diodes. *Mater. Lett.* **2014**, *124*, 129−132.
(61) Chuang, P. H.; Lin, C. C.; Liu, R. S. Emission-Tunable CuInS2/ZnS Quantum Dots: Structure, Optical Properties, and Application in White Light-Emitting Diodes with High Color Rendering Index. *ACS Appl. Mater. Interfaces* **2014**, *6*, 15379−15387.
(62) Haverinen, H. M.; Myllylä, R. A.; Jabbour, G. E. Inkjet Printing of Light Emitting Quantum Dots. *Appl. Phys. Lett.* **2009**, *94*, 073108.

https://doi.org/10.1021/acsphotonics.1c01805
ACS Photonics 2022, 9, 1304−1314

(63) Chen, K. J.; Chen, H. C.; Tsai, K. A.; Lin, C. C.; Tsai, H. H.; Chien, S. H.; Cheng, B. S.; Hsu, Y. J.; Shih, M. H.; Tsai, C. H.; Shih, H. H.; Kuo, H. C. Resonant-Enhanced Full-Color Emission of Quantum Dot-Based Display Technology Using a Pulsed Spray Method. *Adv. Funct. Mater.* **2012**, *22*, 5138−5143.
(64) Zhu, T.; Shanmugasundaram, K.; Price, S. C.; Ruzyllo, J.; Zhang, F.; Xu, J.; Mohney, S. E.; Zhang, Q.; Wang, A. Y. Mist Fabrication of Light Emitting Diodes with Colloidal Nanocrystal Quantum Dots. *Appl. Phys. Lett.* **2008**, *92*, 023111.
(65) Nguyen, T. C.; Can, T. T. T.; Choi, W.-S. Electrohydrodynamic Jet-Sprayed Quantum Dots for Solution-Processed Light-Emitting-Diodes. *Opt. Mater. Express* **2018**, *8*, 3738−3747.
(66) Kim, T.-H.; Cho, K.-S.; Lee, E. K.; Lee, S. J.; Chae, J.; Kim, J. W.; Kim, D. H.; Kwon, J.-Y.; Amaratunga, G.; Lee, S. Y.; et al.*et al.* Full-Colour Quantum Dot Displays Fabricated by Transfer Printing. *Nat. Photonics* **2011**, *5*, 176−182.
(67) Kong, Y. L.; Tamargo, I. A.; Kim, H.; Johnson, B. N.; Gupta, M. K.; Koh, T.-W.; Chin, H.-A.; Steingart, D. A.; Rand, B. P.; McAlpine, M. C. 3D Printed Quantum Dot Light-Emitting Diodes. *Nano Lett.* **2014**, *14*, 7017−7023.
(68) Konstantatos, G.; Sargent, E. H. *Colloidal Quantum Dot Optoelectronics and Photovoltaics*; Cambridge University Press, 2013.
(69) Bahmani Jalali, H.; Melikov, R.; Sadeghi, S.; Nizamoglu, S. Excitonic Energy Transfer within InP/ZnS Quantum Dot Langmuir-Blodgett Assemblies. *J. Phys. Chem. C* **2018**, *122*, 11616−11622.
(70) Bahmani Jalali, H.; Sadeghi, S.; Baylam, I.; Han, M.; Ow-Yang, C. W.; Sennaroglu, A.; Nizamoglu, S. Exciton Recycling via InP Quantum Dot Funnels for Luminescent Solar Concentrators. *Nano Res.* **2021**, *14*, 1488−1494.
(71) Bahmani Jalali, H.; Karatum, O.; Melikov, R.; Dikbas, U. M.; Sadeghi, S.; Yildiz, E.; Dogru, I. B.; Ozgun Eren, G.; Ergun, C.; Sahin, A.; Kavakli, I. H.; Nizamoglu, S. Biocompatible Quantum Funnels for Neural Photostimulation. *Nano Lett.* **2019**, *19*, 5975−5981.
(72) Won, Y. H.; Cho, O.; Kim, T.; Chung, D. Y.; Kim, T.; Chung, H.; Jang, H.; Lee, J.; Kim, D.; Jang, E. Highly Efficient and Stable InP/ZnSe/ZnS Quantum Dot Light-Emitting Diodes. *Nature* **2019**, *575*, 634−638.
(73) Shen, H.; Gao, Q.; Zhang, Y.; Lin, Y.; Lin, Q.; Li, Z.; Chen, L.; Zeng, Z.; Li, X.; Jia, Y.; Wang, S.; Du, Z.; Li, L. S.; Zhang, Z. Visible Quantum Dot Light-Emitting Diodes with Simultaneous High Brightness and Efficiency. *Nat. Photonics* **2019**, *13*, 192−197.
(74) Erdem, O.; Foroutan, S.; Gheshlaghi, N.; Guzelturk, B.; Altintas, Y.; Demir, H. V. Thickness-Tunable Self-Assembled Colloidal Nanoplatelet Films Enable Ultrathin Optical Gain Media. *Nano Lett.* **2020**, *20*, 6459−6465.
(75) Song, J.; Wang, O.; Shen, H.; Lin, Q.; Li, Z.; Wang, L.; Zhang, X.; Li, L. S. Over 30% External Quantum Efficiency Light-Emitting Diodes by Engineering Quantum Dot-Assisted Energy Level Match for Hole Transport Layer. *Adv. Funct. Mater.* **2019**, *29*, 1808377.
(76) Cheng, Y.; Wan, H.; Liang, T.; Liu, C.; Wu, M.; Hong, H.; Liu, K.; Shen, H. Continuously Graded Quantum Dots: Synthesis, Applications in Quantum Dot Light-Emitting Diodes, and Perspectives. *J. Phys. Chem. Lett.* **2021**, *12*, 5967−5978.
(77) Kang, C.; Prodanov, M. F.; Gao, Y.; Mallem, K.; Yuan, Z.; Vashchenko, V. V.; Srivastava, A. K. Quantum-Rod On-Chip LEDs for Display Backlights with Efficacy of 149 Lm W−1: A Step toward 200 Lm W−1. *Adv. Mater.* **2021**, *33*, 2104685.
(78) Jung, S.-M.; Lee, T. H.; Bang, S. Y.; Han, S. D.; Shin, D.-W.; Lee, S.; Choi, H. W.; Suh, Y.-H.; Fan, X.-B.; Jo, J.-W.; et al. Modelling Charge Transport and Electro-Optical Characteristics of Quantum Dot Light-Emitting Diodes. *npj Comput. Mater.* **2021**, *7*, No. 122.
(79) Park, Y.-S.; Roh, J.; Diroll, B. T.; Schaller, R. D.; Klimov, V. I. Colloidal Quantum Dot Lasers. *Nat. Rev. Mater.* **2021**, *6*, 382−401.
(80) Jung, H.; Ahn, N.; Klimov, V. I. Prospects and Challenges of Colloidal Quantum Dot Laser Diodes. *Nat. Photonics* **2021**, *15*, 643−655.
(81) Mueller, S.; Lüttig, J.; Brenneis, L.; Oron, D.; Brixner, T. Observing Multiexciton Correlations in Colloidal Semiconductor Quantum Dots via Multiple-Quantum Two-Dimensional Fluorescence Spectroscopy. *ACS Nano* **2021**, *15*, 4647−4657.
(82) Rahmati, M.; Dayneko, S.; Pahlevani, M.; Shi, Y. Highly Efficient Quantum Dot Light-Emitting Diodes by Inserting Multiple Poly (Methyl Methacrylate) as Electron-Blocking Layers. *Adv. Funct. Mater.* **2019**, *29*, No. 1906742.
(83) Pattison, M.; Hansen, M.; Bardsley, N.; Elliott, C.; Lee, K.; Pattison, L.; Tsao, J. 2019 Lighting R&D Opportunities (DOE/EE-2008). Solid State Lighting Solutions (SSLS) Inc.: Santa Barbara, CA, 2020, DOI: 10.2172/1618035.
(84) European Commission; Directorate-General for Environment; Köhler, A.; Baron, Y.; Gensch, C.; Löw, C.; Moch, K.; Möller, M.; Deubzer, O.; Clemm, C. *Study to Support the Review of the List of Restricted Substances and to Assess a New Exemption Request under RoHS 2 (Pack 15): Final Report* Publications Office, 2021. DOI: 10.2779/47125
(85) European Commission; Directorate-General for Environment; Gensch, C.; Baron, Y. *Assessing Three Exemption Requests for the Use of Cadmium in Quantum Dot Applications in Displays and Lighting: Study to Support the Review of the List of Restricted Substances and to Assess a New Exemption Request under RoHS (RoHS Pack 15-Task 5, Final)*; Publications Office, 2021. DOI: 10.2779/268976
(86) He, P.; Shi, Y.; Meng, T.; Yuan, T.; Li, Y.; Li, X.; Zhang, Y.; Fan, L.; Yang, S. Recent Advances in White Light-Emitting Diodes of Carbon Quantum Dots. *Nanoscale* **2020**, *12*, 4826−4832.
(87) Zhao, B.; Tan, Z. Fluorescent Carbon Dots: Fantastic Electroluminescent Materials for Light-Emitting Diodes. *Adv. Sci.* **2021**, *8*, No. 2001977.
(88) Press, D. A.; Melikov, R.; Conkar, D.; Firat-Karalar, E. N.; Nizamoglu, S. Fluorescent Protein Integrated White LEDs for Displays. *Nanotechnology* **2016**, *27*, 45LT01.
(89) Sadeghi, S.; Melikov, R.; Conkar, D.; Firat-Karalar, E. N.; Nizamoglu, S. Ultra-Efficient and High-Quality White Light-Emitting Devices Using Fluorescent Proteins in Aqueous Medium. *Adv. Mater. Technol.* **2020**, *5*, 2000061.

Recommended by ACS

Tailoring Nanostructures of Quantum Dots toward Efficient and Stable All-Solution Processed Quantum Dot Light-Emitting Diodes
Lixi Wang, Dewei Zhao, *et al.*
APRIL 08, 2021
ACS APPLIED MATERIALS & INTERFACES
READ

Red, Green, and Blue Microcavity Quantum Dot Light-Emitting Devices with Narrow Line Widths
Lishuang Wang, Xingyuan Liu, *et al.*
APRIL 24, 2020
ACS APPLIED NANO MATERIALS
READ

Ultrafast Colloidal Quantum Dot Infrared Photodiode
Qiwei Xu, Xihua Wang, *et al.*
APRIL 28, 2020
ACS PHOTONICS
READ

Quantum Dot–Block Copolymer Hybrids for Low Scattering Luminescent Solar Concentrators
Kayla C. Koch, David A. Rider, *et al.*
APRIL 22, 2022
ACS APPLIED POLYMER MATERIALS
READ

Get More Suggestions >